IIETA International Information and Engineering Technology Association
Advancing the World of Information and Engineering

Revue des Composites et des Matériaux Avancés-Journal of Composite and Advanced Materials
Vol. 34, No. 4, August, 2024, pp. 513-526
Journal homepage: http://iieta.org/journals/rcma

Nanofibers Membrane Loaded with Titanium Oxide and Rifampicin as Controlled Drug Delivery System for Wound Dressing Applications

Dalia Mohammed Jomaa*, Abbas Kamas Hussien, Jamal Jalal Dawood

Materials Engineering, University of Technology-Iraq, Baghdad 000694, Iraq

Corresponding Author Email: Dalia.M.Gomaa@uotechnology.edu.iq

https://doi.org/10.18280/rcma.340413

Received: 27 March 2024
Revised: 10 June 2024
Accepted: 12 July 2024
Available online: 27 August 2024

Keywords:
composite nanofibers, taguchi method rifampicin, local drug delivery, k wound dressing

ABSTRACT

Fibroblast proliferation and microbial infection control play a major role in the efficacy of wound healing. In order to address this, we created dressing membranes by loading polyvinyl alcohol/chitosan with Rifampicin (RIF) and titanium oxide (TiO_2). Using the Taguchi technique, a four-level experimental design procedure (L16) was used to optimize the mechanical parameters. These biomaterials have desirable mechanical properties, are antimicrobial, and have high compatibility with human tissues, which makes them useful for a range of biomedical applications. In order to create composite nanofibers of polyvinyl alcohol/chitosan with TiO_2, this study effectively used electrospinning. Using a variety of methods, such as field emission scanning electron microscopy (FESEM), Fourier transform infrared spectroscopy (FT-IR), wettability testing, swelling tests, degradation tests, and nanoindentation tests, the resulting composite nanofibers were thoroughly characterized. The morphological study showed that the structures were clearly defined and had sizes between 48 and 276nm. Methyl thiazolyl tetrazolium (MTT) assays were used in in vitro evaluations to assess the biocompatibility and capacity to promote cell proliferation of the polyvinyl alcohol/chitosan composite nanofibers. Additionally, when compared to polyvinyl alcohol/chitosan nanofibers, the composite nanofibers demonstrated improved antibacterial activities in drug-loaded samples and demonstrated excellent bactericidal activity against both Gram-positive and Gram-negative bacteria. After the mechanical properties of each specimen were evaluated, the important elements influencing these mechanical properties were found and screened using the Taguchi orthogonal array L16 design. Therefore, the composite nanofibers of polyvinyl alcohol and chitosan show promise for use in wound dressings.

1. INTRODUCTION

For people with type-2 diabetes, impaired wound healing is a serious medical concern because it can lead to chronic wounds and foot ulcers, which increase medical costs and lower quality of life. Diabetes-related wounds can cause long-lasting, excruciating consequences that are typified by microbial infections, decreased growth factor secretion, disturbed angiogenesis, and extended chronic inflammation. These long-term, non-healing wounds often worsen the situation and require repeated hospital stays, which increases the risk of amputation of the afflicted limb or organ [1]. To promote cell adhesion and proliferation, the ideal scaffold for wound dressing should resemble the composition and properties of skin tissue. It should provide mechanical strength to hasten the healing process and successfully isolate the site from adverse conditions to prevent subsequent injury [2].

Many biopolymer scaffolds have been developed as essential components for a range of biomedical uses, such as controlled drug delivery, tissue engineering, and developing biomedical technologies like regenerative medicine. In medical settings, Among the often-utilized biomaterials include polymers like polylactides, chitosan, polyvinyl alcohol, polyglycolide, polydioxanone, and polycaprolactone.

TiO_2-reinforced polyvinyl alcohol and chitosan are used in this work [3].

As a naturally occurring cationic polysaccharide, chitosan has attracted a lot of interest due to its biodegradability, renewability, non-toxicity, and functionality. As such, it is a versatile biopolymer with a wide range of uses, mostly in the food, cosmetics, and pharmaceutical industries. Chitosan has been widely studied in the medical field. It is used as absorbable surgical sutures, artificial skin, and wound healing accelerators. It is also used as a novel physiological material because of its antitumor, immunoenhancing, antimicrobial, and hypocholesterolemia qualities [4].

Polyvinyl alcohol (PVA) is a significant synthetic polymer with a history lasting over 90 years. Because of its ability to form films, PVA, which is created by saponifying poly (vinyl acetate), has been blended with other natural polymers for a considerable amount of time. PVA's fundamental limitations prevent it from dissolving completely in water [5].

Since it is regarded as the second generation of nanotechnology. The recent incorporation of nanotechnology into biomaterials has received significant attention. Biomaterials encompass the arrangement of hetero- or homo-nanomaterial structures for many different uses. The use of metal oxide nanoparticles with biopolymers to create novel functionalities and improve their properties is made possible by the use of nanocomposites in nanotechnology [6].

In particular, metal oxide nanoparticles show exceptional features in wound dressing applications, including biocompatibility and antimicrobial activities, indicating tissue regeneration. The white solid inorganic substance titanium dioxide (TiO_2) is the tenth most prevalent element in the world. The mechanical properties, excellent corrosion resistance, biocompatibility, and enhanced antibacterial efficiency against both Gram-positive and Gram-negative bacteria are all significantly impacted by the size of TiO_2 nanoparticles. TiO_2 nanotube materials have been thoroughly studied as drug delivery platforms, inhibiting bacterial adherence, and promoting adhesion and growth in tissue regeneration. An earlier study developed a bilayer film and composite with TiO_2 nanostructures for use in wound healing. According to their findings, adding TiO_2 nanostructures to chitosan and pectin enhanced their tensile strength, showed remarkable antibacterial activity, had acceptable biocompatibility, and sped up wound healing [7].

The unique characteristics of TiO_2, PVA, and chitosan nanoparticles have led us to investigate the feasibility of combining these elements to produce an effective nano-dressing material for wound healing applications. Furthermore, water or secretions from wounds may cause nanoparticles to disassemble, opening the door for assaults on microbial cell membranes. Our current study demonstrated the additive effects of a ternary nano dressing composed of chitosan, PVA, and TiO_2. It demonstrated improved antibacterial properties, a contact-active surface, compatibility with cell lines, excellent hydrophilic behaviour, and a faster healing effect when compared to the control in wound healing.

An important concept change in the fields of drug delivery and human applications can be seen in biomaterials.

Their versatility and adaptability have not only improved therapeutic outcomes but have also greatly decreased the burden of side effects. This study provides a complete overview of biomaterials, with a focus on their critical role in medication administration, classifying them according to their biobased, biodegradable, and biocompatible nature, and highlighting their properties and benefits. [8]

Limitations relative to this application are structural morphology fabrication technique, characteristics, and efficiency. Frequently, film, membranes, and fibres exhibit favorable oxygen permeability and sturdy mechanical qualities. Sponges and hydrogel structures have the capacity to absorb substantial quantities of exudate, preserve a moist environment, and serve as carriers for bioactive chemicals and cells. The use of these biomaterials is contingent upon their morphology [5, 6].

A statistical technique called the Taguchi design of experiments aims to minimize the number of tests required to evaluate the impact of various parameters on both the quantity and quality of a product. Additionally, by effectively removing the factors that are most important to the reaction and disregarding the others, this technique creates the most favorable conditions [8].

The Taguchi factor design methodology is a cost-effective way to improve production procedures and meet high-quality objectives without spending extra money. The impact of disturbance components on the desired properties of a system or signal is measured by the signal-to-noise ratio, or S/N ratio. Multiple variables can be examined with an orthogonal array (OA), reducing the number of tests required. Three performance criteria are used to evaluate the signal-to-noise (S/N) ratio: maximization, minimization, and nominal optimization. The multiple data points in a laboratory setting are combined using the signal-to-noise ratio based on the particular characteristic that has been studied. [9]

This study involves the fabrication of PVA/CS/NanoTiO_2 composite electrospun membranes using the electrospinning technique. This technology is economical and allows for the production of wound dressings with various nanofibers and customisable pore shapes. These dressings have high porosity, excellent swelling capacity, and promote cellular adhesion. Additionally, they create a moisture and warmth environment that accelerates the wound healing process, which is done when TiO_2-loaded PVA/CS have been produced to improve. The physical characteristics of the produced nanofibers were examined, followed by the addition of RIF as an antibiotic to enhance wound healing. The assessment comprised mechanical testing, evaluation of swelling qualities, and an antibacterial test. The objective is to examine the biocompatibility qualities, drug release profile, and cytotoxicity effects on human epidermal cells of the electrospun nanocomposites that were created.

The objective of this project is to fabricate nanofibrous scaffolds using chitosan and polyvinyl alcohol, reinforced with titanium dioxide, and enhanced with Rifampicin (RIF). These materials will be applied as bio-nanocomposite materials. Furthermore, the Taguchi method will be employed for carrying out experiments and assess the effects of different parameters. The aim is to improve the choosing of important factors that affect mechanical characteristics and achieve the required morphology for wound dressings.

2. MATERIALS AND TECHNIQUES

2.1 Materials

Materials used in this research are Chitosan (CS, with M.W. 161g/mol molecular weight) was purchased from Glentham (United Kingdom). Poly (vinyl alcohol) 124 (PVA-124, 88% hydrolyzed, Mw~67,000), Astic Acid 98-100% from Merck and Nano titanium dioxide, were purchased from Sky Spring Nanomaterials (USA), phosphate buffer saline (PBS), pH=7.4 The lysozyme (LZ) obtained from Sigma (USA) has a protein content of at least 90% and an activity level of at least 40,000 U/mg. The CDH (India) is the source of this product.

2.2 Preparation of PVA/Chitosan solutions

To prepare a nanofiber membrane with an electrospinning device, dissolve eight percent polyvinyl alcohol (PVA) in distilled water at 60 degrees Celsius. This is the first step in the preparation process. After that, the mixture is agitated for two hours. Furthermore, a solution with a 2% weight percent chitosan concentration was made by dissolving chitosan (CS) in a solution containing 2% weight of acetic acid. By combining liquids in a weight ratio of 85-15 weight percent and adding TiO_2 NP at three distinct concentrations (0.2, 0.4, and 0.6), the PVA-CS ratio was ascertained.

For an hour, the solution was constantly stirred. First of all,

the makeup of the samples is explained in depth in this document. With this particular mix, electrospun fiber synthesis was carried out. This membrane was made using electrospinning apparatus, which involved pumping a polymer solution into a needle gauge 18 from a 10mL syringe. There was an 18kV voltage. The electrospinning process was run at 22±2℃, room temperature. A 12.5cm tip-to-collector distance was chosen. A flow rate of 0.5mL/h was used. Table 1 displays the makeup of the film blends after the produced nanofibers were dried at room temperature prior to additional examination.

Table 1. Code samples and their related chemical compositions

No. of Sample	PVA	CS	TiO_2	RIF
1	85	15	0	0
2	85	15	0.2	0
3	85	15	0.4	0
4	85	15	0.6	0
5	85	15	0	50
6	85	15	0.4	50

2.3 Fourier transform infrared spectroscopy

The vibration of functional groups in blended films was measured using FTIR microscopy (Bruker, Germany).

2.4 Characterization of morphology by (FESEM) field emission scanning electron microscopy and (EDX) energy dispersion X-ray spectroscopy

Mira 3-XMU FE-SEM was used to analyze the scaffolds' morphology after they were created. Before being examined with FESEM at 15KV accelerating voltage, the specimens have been gold plated (10nm) through sputtering. Fiber diameter and pore size were quantified in FESEM images using the Image j program.

2.5 Wettability test

When a drop of water rests on a lotus leaf, the Contact Angle (CA) it takes is often more than 160 degrees. The term "hydrophobic" has been in use since antiquity to characterize a solid surface's reluctance to hold liquid. The textile business, packaging, coating industry, bio-engineering, electrical devices, and medication delivery are just few of the many fields that might benefit from hydrophobic surfaces [5]. The angle that a liquid creates with a solid, known as the Static Contact Angle, is the most crucial feature in identifying superhydrophobic materials. The surface is hydrophilic if the water static contact angle (CA) is less than 90 degrees, hydrophobic if it is between 90 and 150 degrees, and superhydrophobic if it is greater than 150 degrees [6].

2.6 Degree of Swelling

The swelling degree of blended films was evaluated using the ASTM D4546-08 15 standard. The films were immersed in a phosphate-buffered saline (PBS) solution at pH 7.2 for 24 hours at room temperature. The mixed films were removed once they had become swollen, and the excess solution was drained using filter paper. Eq. (1) was used to determine the degree of swelling.

$$Degree\ of\ swelling(\%) = \frac{(w2 - w1)}{w1} * 100 \quad (1)$$

where, w1, w2 were: weights of dried, swollen samples, respectively.

2.7 Degradation rate

Blended films were immersed in a phosphate-buffered saline (PBS) solution containing lysozyme enzyme at a concentration of 0.0001g/L by ASTM F1635-04a 16. And kept in a 37℃ incubator for a month. Every three days, we would restart the solution. Films were bleached in solution, rinsed in phosphate-buffered saline (PBS), dried, and weighed once weekly.

Degradation rate was determined by the Eq. (2). [10]

$$Weight\ loss\ (\%) = \frac{(w0 - w1)}{w0} * 100 \quad (2)$$

where, w0 is the dry weight before degradation and W1 is the dry weight after degradation.

2.8 Antimicrobial activity

The agar well diffusion assay [11] was used to test the antibacterial properties of the produced Samples (1 to 6) against Gram's negative and Gram's positive bacterial strains. Muller-Hinton (MH) agar, in a volume of around 20mL, was placed sterilely on Petri plates. The bacterial strains were taken from their respective stock cultures with the use of a sterile wire loop [12]. After the organisms were cultured, wells were drilled with a sterile point into the agar plates at a diameter of 6mm. Different concentrations of the Samples (from 1 to 6) were injected into the drilled wells. After incubating the culture plates containing the Samples (1-6) and the test organisms at 37℃ for a full 24 hours, the average diameter of the zones of inhibition were measured and recorded [13].

2.9 In vitro cytotoxicity

The fibroblast vitality on the produced nanofibrous mats was assessed using the MTT test. Under usual conditions of 37℃ and 5% CO_2, the cells were grown in DMEM media supplemented with 10% fetal bovine serum and 1% penicillin/streptomycin antibiotic. Every experiment was run three times for the 24 hours, 48 hours, and 72 hours of culture time that were indicated. We carried out a number of tests in order to improve the appraisal and assessment of biocompatibility [14].

First, we used the MTT to assess the cytotoxicity. Then, using fibroblast (L929) cells and the cell counting kit-8 (CCK-8) method, we assessed the strength and rate of cell division. Compared to MTT, MTS, or XTT, or other tetrazolium salts, the CCK-8 test is more sensitive. With the use of this analytical method, colorimetric assays with a high degree of sensitivity may be used to determine the number of living cells in proliferation tests and evaluate cytotoxicity [15, 16].

The normalized relative viability or cell growth (%) was calculated from the following equation:

For calculation of cell viability [14]:

$$Survival\ rate\% = \frac{AS - AC}{AC} * 100 \quad (3)$$

As: Mean absorbance of each sample

Ac: Mean absorbance control

$$Cytotoxicity\ rate = 100 - Survival\ rate \quad (4)$$

2.10 In vitro drug release

Using UV spectrophotometry at 237nm, the release of rifampicin from samples with and without the addition of nanopowder was investigated. 500 µL of saline phosphate buffer (PBS) was added to two samples per condition, which were then evaluated and put on 24-well plates to assess the release of rifampicin. 500 µL of solution were taken from each well for the absorbance measurement after 1, 4, 24, 48, and 72 hours, and at each time point, fresh PBS was used in place of the release solution. The plates were kept moist and incubated at 37°C in the absence of light to prevent PBS evaporation. Since ε237 nm is equal to 33 200, the released rifampicin was quantified using the Lambert-Beer equation and normalized on 5mg of the membrane [17].

2.11 Mechanical properties

Nanoindentation experiments were conducted using a Hysitron TriboLabs nanomechanical testing system equipped with a two-dimensional force-displacement detector. The transducer has a range of 1-10,000µN and can apply loads with a high load resolution of 1nN. In addition, it records a maximum penetration depth of 3000nm (3µm) and has a resolution of 0.04nm. H and Er values are measured using a three-sided pyramidal Berkovich diamond indenter with a 120nm radius of curvature. Before starting any experiments, fused silica, a reference material, is used for calibration to determine the tip radius (tip area function). The investigations are conducted in a controlled atmosphere with a temperature of 23°C and a relative humidity of around 45% [18].

3. DESIGN OF EXPERIMENTS

The mechanical properties of the (PVA/CA/TiO_2) composite are influenced by five main factors: stiffness content (µN/nm), reinforcement content (g), maximum force (µN), contact area (nm2) and maximum depth (nm), A Taguchi model with four levels is employed for optimizing these parameters and assessing their impact on Hardness. Table 2 presents an overview of the four parameters together with their related answers. The parameters' values are assigned according to the results of an initial inquiry. In order to evaluate the influence of each variable on Hardness, the Signal-to-Noise (S/N) ratios were obtained for each of the four parameters., these variables were chosen because they have a direct effect on the value of hardness when obtained from the nanoindentation test and the value of hardness very important factor when using these membranes as wound dressing materials.

An analysis of variance (ANOVA) is used to assess the statistical significance of the factors that impact hardness, with a confidence level of 95%. Minitab 20 is utilized for implementing the optimization process based on the Taguchi technique. The experiment was conducted using Taguchi's Orthogonal Array (Taguchi-OA), which consisted of level-4 and parameter-4 combinations, necessitating sixteen runs.

Table 2. Experimental parameters (factors) and their levels

Level	Samples	Reinforcement Content (g)	Contact Stiffness (µN/nm)	Max Force(µN)	Max Depth(nm)	Contact Area nm^2
1	(CS+PVA)+0.2TiO_2	0.2	7.8	179.0	124.2	5.99
2	(CS+PVA)+0.4TiO_2	0.4	6.5	185.6	92.2	3.48
3	(CS+PVA)+0.6TiO_2	0.6	5.5	147.2	289.3	3.06
4	(CS+PVA)+0.4TiO_2+Rif	0.4	1.3	113.6	468.7	6.64

4. RESULTS AND DISCUSSION

4.1 Fourier-transform infrared (Ftir) analysis

The FTIR spectra recorded from the samples are shown in Figure 1. Figure 1 (A) displays the unmixed chitosan spectrum. N-H and C-H stretching are responsible for the peaks at 2922.87 and 2874.07cm. The N-H stretching in amide II is responsible for the peak at 1630.38cm. The characteristic PVA spectrum is clearly seen in Figure 1 (B).

Bonds between oxygen and hydrogen (at 2946.71cm) and carbon and hydrogen (at 2879.52cm) produce those spectral bands. As can be seen in Figure 1 (C) [18] when chitosan is added to PVA, a new peak appears at 1721.82cm, indicating interaction between O-H (for PVA) and N-H (for chitosan).

As can be seen in Figure 2, The improved properties of the mix can be due to the interactions between chitosan and PVA, specifically the aggregation of side chains with hydrophobic properties and the formation of intermolecular and intramolecular hydrogen bonds. [19, 10].

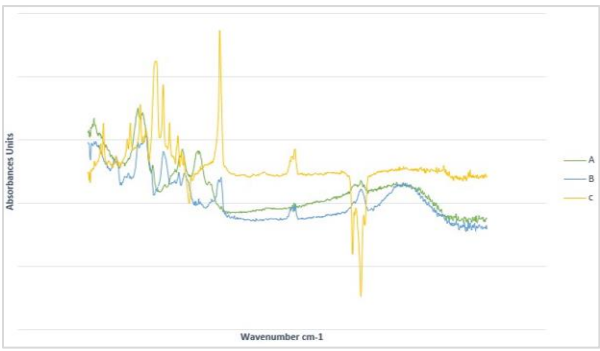

Figure 1. Fourier Transform Infrared Spectroscopy (FTIR) Analysis A) cs; B) PVA; C) PVA+cs

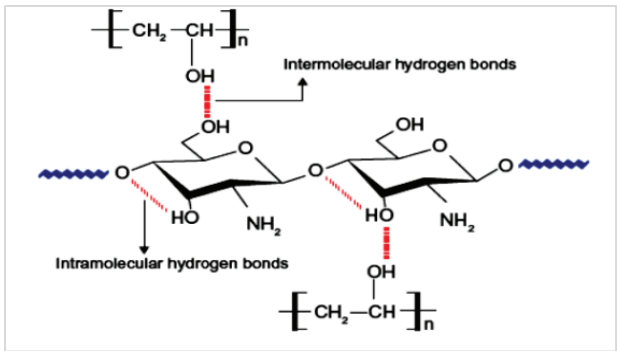

Figure 2. CS and PVA interaction [10]

From Figure 3, all of the expected peaks could be seen clearly once TiO_2 was included, demonstrating that the two materials are chemically compatible [20]

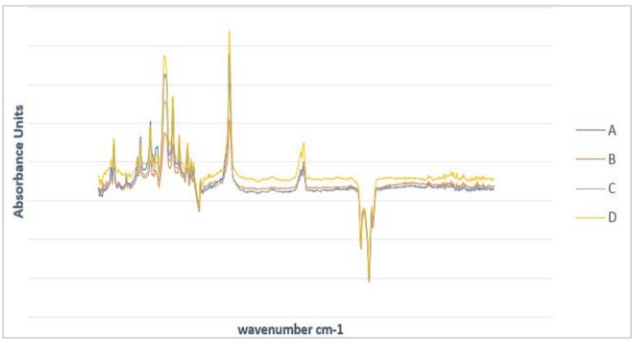

Figure 3. Fourier Transform Infrared Spectroscopy (FTIR) Analysis: A) PVA+CS; B) PVA+CS/0.02TiO_2; C) PVA+CS/0.04TiO_2; D) PVA+CS/0.06TiO_2

4.2 Nanofiber diameter and distribution

The PVA/CS exhibits an average pore size of 267.064nm and an average fiber diameter of 48.093nm that illustrated in Figure 4 (a). The FESEM micrographs of the PVA/CS nanofiber modification with TiO_2 nanoparticle addition are displayed in Figures 4 (b) and (c). The fiber's morphology remained unchanged upon the addition of TiO_2 nanoparticles; it exhibited a distinctive ribbon structure with few bead defects. The average fiber diameter and pore size of PVA/CS+0.02 TiO_2 were measured at 126.466nm and 277.105nm, respectively. Figure 4 (c) show FESEM micrographs of the PVA/CS+TiO_2 0.4gm, which exhibit an increase in fiber diameter as a result of the particle embedding and the random distribution of TiO_2 particles among PVA: CS fibers, average fiber diameter (100.157) nm and the average pore size (620.463) nm.

Figure 4 (d) show the FESEM micrographs of the PVA/CS+TIO_2 0.6gm, Since the particles in this scenario are nanometric in size, they have a greater propensity to agglomerate and adhere in the form of aggregates to the polymeric fibres, which has a detrimental impact on the sample's homogeneity across broad regions, the average fibre diameter of PVA/CS modification is (267.1659) nm and the average pore size to be (559) nm.

FESEM micrographs of the (PVA/CS nanofibers) +RIF can be shown in Figure 4 (e). The inclusion of RIF in composite nanofibers significantly reduced the diameter of PVA nanofibers, average fibre diameter is (57) nm for the PVA/CS blend+RIF, across all layers, the morphology reveals a web of random, non-woven, one-dimensional polymeric structures [21]. the potential for a reduction in nanofiber width due to the incorporation of polar components, with an average pore size of 831.591nm.

Figure 4 (f) shows the FESEM micrographs of the PVA/CS+TiO_2 0.4gm+RIF, an average fibre diameter of PVA/CS+TiO_2 0.4gm+RIF modification, was found to be (133.3407) nm, that means increase fibre diameter when computation because adding TiO_2 as nanoparticles. with average pore size (336.916) nm [22].

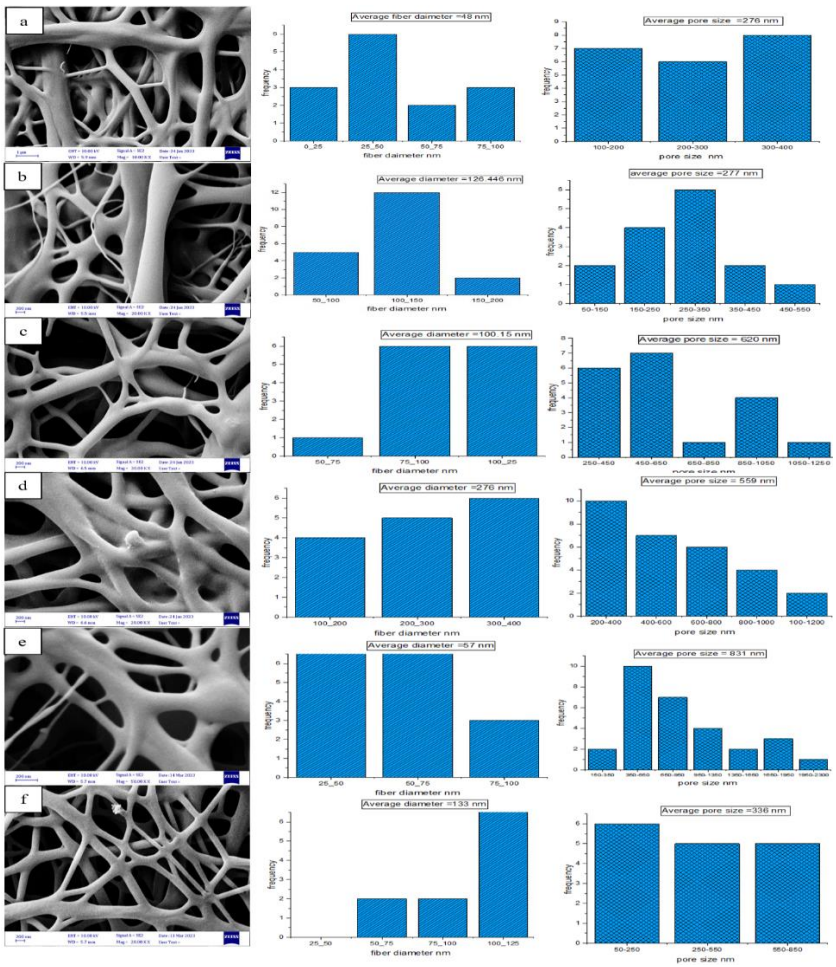

Figure 4. Fiber diameter and pore size of A) PVA+CS; B) PVA+CS/0.2TiO_2; C) PVA+CS/0.4TiO_2; D) PVA+CS/0.6TiO_2; E) PVA+CS+RIF; F) PVA+CS+0.4TiO_2+RIF

4.3 Wettability test

All the contact angle data was the average of seven readings taken at various positions on the surface, and the water contact angles were determined using the low bond axisymmetric drop shape analysis technique [10] The surface was splattered with a single drop of water. A high-speed CCD camera was used to record this procedure at 35 frames per second [23].

Figure 5 displays the contact angle values of PVA+CS (about 75° degrees). Because TiO_2 is hydrophilic, the contact angle values for (PVA+CS) TiO_2 were reduced. After 10 minutes, observed values of (60°) were seen for (PVA+CS) TiO_2, when liquid was released over these nanofibrous scaffolds. Contact angles were reduced, although only slightly, in a (PVA+CS) TiO_2+RIF nanofibrous scaffold. The value dropped to (55°) degrees.

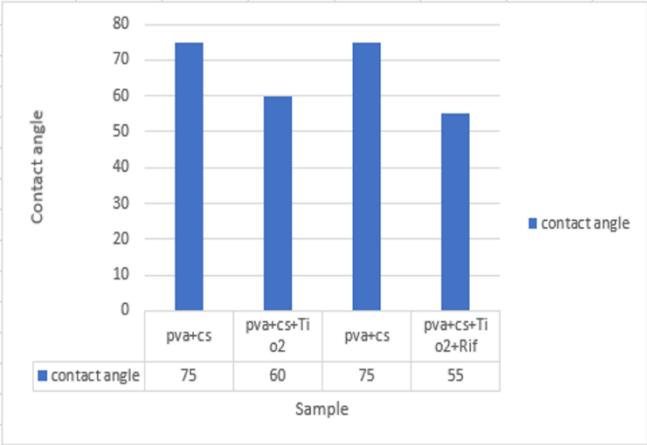

Figure 5. Scaffold standard deviations of contact angle values

4.4 Antibacterial activity

The data were statistically analyzed using GraphPad Prism [24]. The average and standard deviation (mean ± SD) of three different tests is used to illustrate the data. Indicate a significant difference at the 0.05 significance level ($p<0.05$) [25]. The results of antibacterial activity at various concentrations are shown in Table 3, illustrated the inhibition zone against E. coli bacteria.

Table 3. Antibacterial activity (inhibition zone)

Sample	E. coli
(CS+PVA)	10
(CS+PVA)+0.2TiO_2	12
(CS+PVA)+0.4TiO_2	13
(CS+PVA)+0.6TiO_2	14
(CS+PVA)+RIF	11
(CS+PVA)+0.4TiO_2+RIF	22

4.5 The swelling tests

Figure 6 displays the results of testing that are noted increasing swelling capacity for the membrane when TiO_2 as a nanoparticle because the increasing surface area means increased absorption of water then promotes a higher swelling rate, and TiO_2-NPs in the membrane is hydrophilic, which is important to assist for quick absorption of exudates. Better absorption of exudates will keep wounds dry and prevent airborne infection [24, 26].

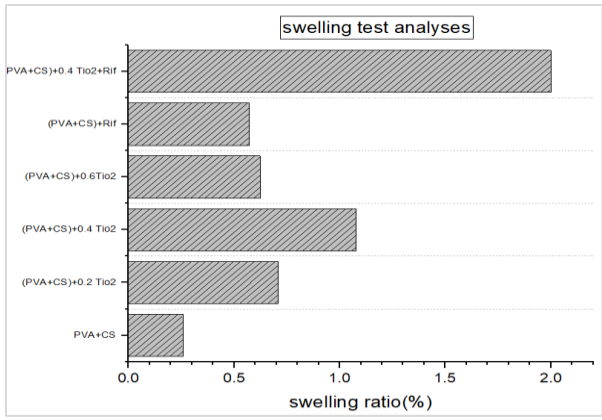

Figure 6. Swelling tests analyses

4.6 Degradation test

Decomposition should occur and new skin is produced. Cross-linked TiO_2 degradation of (PVA+CS). Tissue engineering relies heavily on in vitro biodegradation as a measuring stick. For the enzyme to degrade the film, it must penetrate the film's surface and react with the polymer mixture.

It is evident from the data that the PVA/CS membrane degrades more quickly than the PVA/CS/TiO_2 membrane. This is because the addition of TiO_2 nanoparticles to the polymer matrix strengthens it, giving the membrane reinforcement and rigidity [27, 28].

After one week, two weeks, and three weeks in PBS medium, all of the as-fabricated bandages degraded by 24-45%, 39%-48%, and 45-70%, respectively. TiO_2NPs slowed down the pace at which the composite bands degraded. This may be the reason why TiO_2NPs react with CS/PVA bandages [29] shown by the Figure 7.

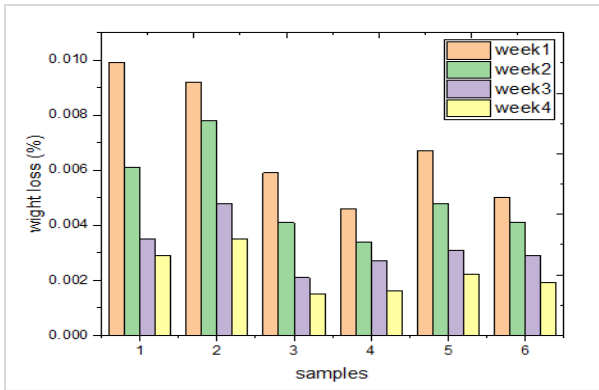

Figure 7. Weight loss of samples

4.7 Cell viability

The evaluation of viable fibroblasts was accomplished using the MTT assay, which assessed the in vitro cell proliferation across six separate samples. Figure 8 shows the cell viability on different nanofibrous samples at 24 hours, 48 hours, and 72 hours.

Cell culture plates without any nanofibrous material were used as controls. Significantly, compared to the control cultures (cells grown on the plastic surface of the culture plate), the proliferation and vitality of L929 cells on the membranes exceeded those in the former. Furthermore, it was noted that fibroblast cells showed the highest proliferation and survivability of all the created composite membranes. The

greater surface area accessible on composite membranes in comparison to standard cultures may be the cause of this improved responsiveness. However, the cell attachment was significantly increased for all the mentioned periods and that indicates no-cytotoxic excretion for all membranes [30, 31].

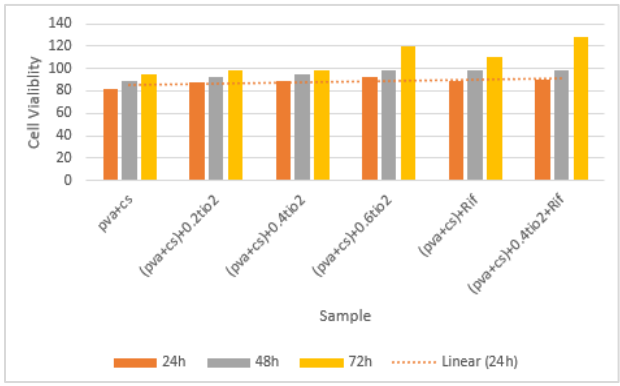

Figure 8. MTT assay for the evaluation of viability of cells cultured on the samples

4.8 Drug release properties of RIF loaded (PVA+CS) and (PVA+CS)+TiO_2 nanofiber membranes

Since Rif, CS, PVA, and TiO_2 are water-soluble compounds, they can be rapidly dissolved in aqueous solutions, leading to a significant initial bursting at short periods. It reached equilibrium two hours into the release. The inner medicines eventually diffused to the buffer solutions through the carrier as the PVA+CS+TiO_2 nanofiber membranes swelled in the buffer solutions and finally reached release equilibrium. Due to the ability of TiO_2 nanoparticles to influence drug delivery, RIF release is greater when a drug is loaded in (PVA+CS)+TiO_2+RIF compared to (PVA+CS)+RIF (as shown in Figure 9) [32].

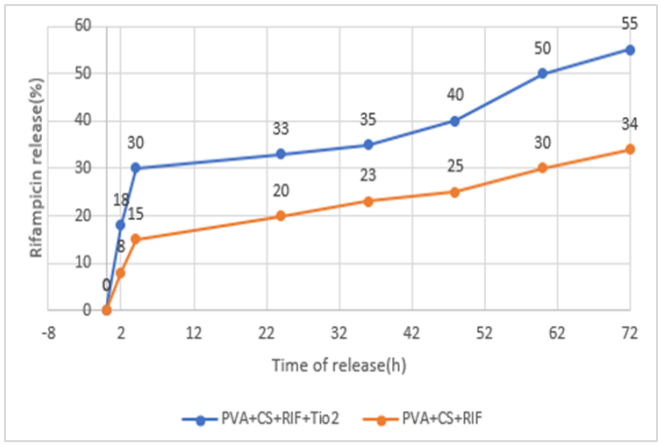

Figure 9. Rifampicin release kinetic from (PVA+CS) and (PVA+CS)+TiO_2 membrane

4.9 Analysis of the samples using nanoindentation

To treat burn wounds, many synthetic and natural polymer materials have been developed; however, as Table 4 illustrates, their use is frequently limited by their poor mechanical qualities and slow rates of water absorption. In the context of treating burn wounds, improvements in mechanical qualities have been put into place to overcome these constraints.

In this study nanoindentation tests can be noticed in the elongation-force curve, which is equivalent to the Stress-strain curve in Figures 10 and 11. The load-unload curves for the chitosan (CS), polyvinyl alcohol (PVA), and chitosan-polyvinyl alcohol (CS+PVA) are shown in Figure 10, It is seen that increased Mechanical properties through blend Cs with PVA. When compared with cs alone and in Figure 11 observed adding 0.2wt.% TiO_2, caused an increase in Mechanical properties, it is noticed that by adding TiO_2 to the CS+PVA membrane, the mechanical properties will increase [33, 34].

Table 4. Mechanical properties of the sample

Sample	Er(Gpa)	Hardness(Gpa)	Contact Stiffness (μN/nm)	Max Force (μN)	Max Depth(Nm)	Contact Area(nm^2)
CS	6.5	0.20	6.8	175	151.6	2.11
PVA	1.3	0.17	1.4	160.1	225.2	1.32
CS+PVA	8.9	0.30	7.8	179.0	124.2	5.99
(CS+PVA)+0.2 TiO_2	10	0.55	6.5	185.6	92.2	3.48
(CS+PVA)+0.4 TiO_2	2.8	0.05	5.5	147.2	289.3	3.06
(CS+PVA)+0.6 TiO_2	0.4	0.02	1.3	113.6	468.7	6.64

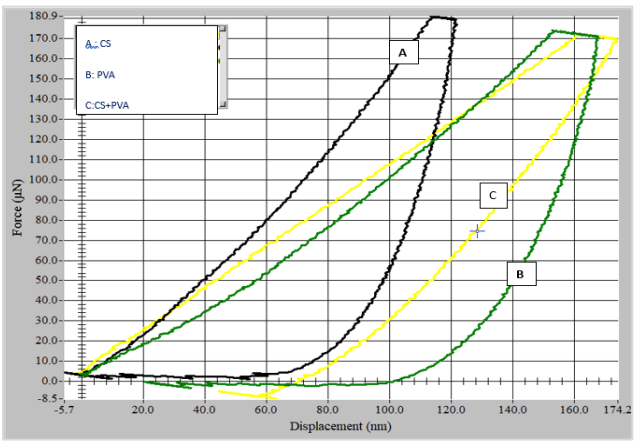

Figure 10. Load-unload curves at A: (CS); B: (PVA); C: CS+PVA)

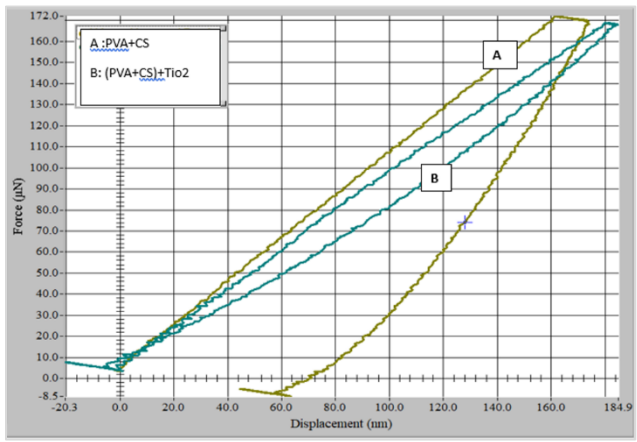

Figure 11. Load-unload curves at A: (CS+PVA); B: (CS+PVA)+TiO_2

It is clear from Figure 12, which shows lowered modulus and hardness, that adding less TiO_2 nanoparticle content causes the membranes' hardness to climb as TiO_2 content does.

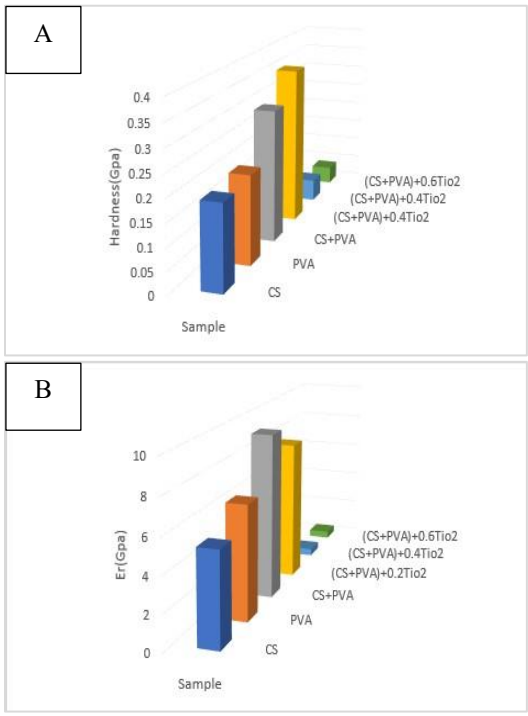

Figure 12. A: Hardness values of samples; B: reduced modulus (Er) values of samples.

Up to 0.2 weight per cent of TiO_2, the composite's increased decreased modulus shows a linear increase. However, the hardness of the (PVA+CS)+nTiO_2 nanocomposite membranes decreases with additional increases in TiO_2 nanoparticle content (0.4 and 0.6 wt.%). A lower weight % of TiO_2 nanoparticles has a more noticeable reinforcing effect, increasing the tensile modulus and preventing polymer stretching.

When compared to the pure (PVA+CS) membrane, the (PVA+CS) membrane containing 0.2 weight per cent TiO_2 nanoparticles exhibits greater hardness [35]. This is explained by the fact that the high surface energy of the nanoparticles causes them to aggregate easily, leading to poor dispersion in the polymer matrix. This tendency becomes much more pronounced with an increase in TiO_2 content, which causes TiO_2 aggregates to develop inside the polymer matrix. By serving as concentration points for tension, these aggregates prevent stress from moving from the polymer matrix to the fillers. As a result, the dispersion of TiO_2 in the (PVA+Cs) polymer matrix is more uniform at lower percentages of TiO_2 concentration. The result is enhanced mechanical properties, including a more even distribution of stress, a decrease in the formation of stress-concentration points, and an increase in the contact area for stress transfer between fillers and the polymer matrix [7].

4.10. Taguchi results

4.10.1 (DOE) Design of experimental

Four distinct experiments are carried out for each test condition in a total of 16. Trials containing experiments under the previously mentioned parameters. The Hardness findings and decreased modulus (Er) are displayed in Table 4.

The smaller-the-best principles, which are utilized to assess the ideal condition connected to the lowest hardness value, were included in the research. The graphical representations presented in Figure 13 are employed to determine the optimal set of parameters. Based on these charts, the maximum force (µN) at level 4 (185.6µN) produced the most successful result, the contact area (3.06) at level 1, the control factor of Reinforcement (g) at level 3 (0.6) produced the best result, and the contact stiffness (µN/nm) control factor (7.8) produced the best result at level 4 max depth (124.2nm) at level 2, and Figure 14 displayed Response Optimisation hardness (Gpa) [36].

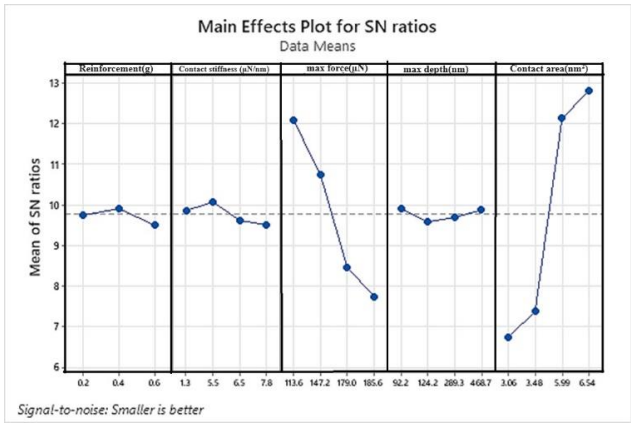

Figure 13. Taguchi Inspection: Main effects plot for Hardness: smaller is better

On the other hand, the greatest modulus of elastase Er-which would be the ideal condition for this study-is found using the greater is better criteria. The best combination of parameters is found using the charts in Figure 14. Based on these charts, the best outcome was obtained with the control factor of Reinforcement (g) at level 1 (0.2). While the maximum depth (468.7nm) at level 4, the maximum force (µN) at level 1 (113.6µN) offered the best result, and the contact area (3.06) at level 1, Figure 13 shows the respond optimization modulus of elastase Er (Gpa), the contact stiffness (µN/nm) control factor (7.8) gave the best result at level 4.

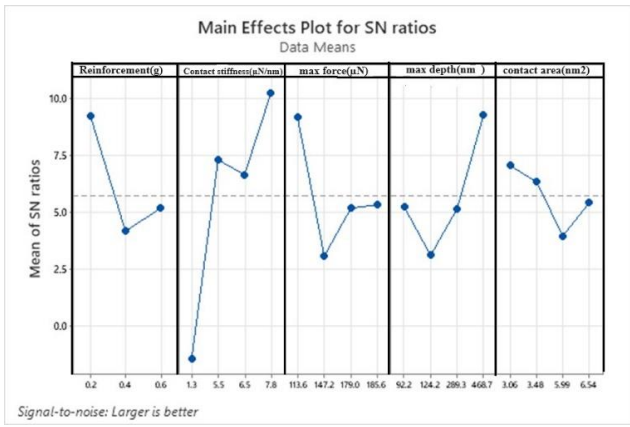

Figure 14. Taguchi Analysis: Main effects plot for Mean of Means for Er smaller is better

4.10.2 Analysis of Variance (ANOVA)

A study was conducted to determine the process parameters that have significant effects on the response variable. The error sum of squares was combined and the findings of the Hardness and elastic modulus Er test percentage were examined using

an ANOVA method. The factors and levels in designing a factorial design are summarized in supplementary Table 5 and Table 6 [37], the model created by analysis of variance (ANOVA) in Eq. (5) for Hardness and Eq. (6) for elastic modulus. Table 7 illustrated Taguchi L16 orthogonal array of designed experiments.

Regression Equation

$$\begin{aligned}\text{Hardness}=a0-a1\times 1\ 92.2+a2\times 1\ 124.2+a3\times 1\ 289.3\\ -a4\times 1\_468.7+b1\times 2\_3.06+b2\times 2\_3.48--b3\times 2\_5.99-\\ b4\times 2\_6.54-c1\times 3\_113.6-c2\times 3\_147.2+c3\times 3\_179.0\\ +c4\times 3\_185.6+d1.\times 4\_1.3-d2\times 4\_5.5+d3\times 4\_6.5\\ -d4\times 4\_7.8+.\ e1\times 5\_0.2-e2\times 5\_0.4+e3*\times 5\_0.6\end{aligned} \quad (5)$$

A: max depth(nm); B: contact area(nm^2); C: max force(μN); D: contact stiffness(μN/nm); E: reinforcement content (g).

$$\begin{aligned}\text{Elastic modulus. Er}=a0+a1\times 1\_92.2-a2\times 1\_124.2-a3\\ \times 1\_289.3+a4\times 1\_468.7+b1\times 2\_b1b1\times 2\_3.48-b1\\ \times 2\_5.99-b2\times 2\_6.54+c1\times 3\_113.6-c2\times 3\_147.2-c3\\ \times 3\_179.0-c4\times 3\_185.6-d1\times 4\_1.3+d2\times 4\_5.5+d3\\ \times 4\_6.5+d4\times 4\_7.8+e1\times 5\_0.2-e2\\ \times 5\_0.4-e3\ \times 5\_0.6\end{aligned} \quad (6)$$

A: max depth(nm); B: contact area(nm^2); C: max force(μN); D: contact stiffness(μN/nm); E: reinforcement content (g).

Table 5. Component of Eq. (3)

Variable	Constant	Constant	Constant	Constant	Constant
A(×1)	-a0(0.3520)	-b1(0.1425)	-c1(0.0879)	-d1(0.0241)	-e1(0.0015)
B(×2)	-a1(0.0056)	-b2(0.0950)	-c2(185.6)	-d2(0.0309)	-e2(0.0155)
C(×3)	-a2(0.0086)	-b3(0.1050)	-c3(0.0461)	-d3(0.0169)	-e3(0.0140)
D(×4)	-a3(0.0001)	-b4(0.1325)	-c4(0.0849)	-d4(0.0101)	
E(×5)	-a4(0.0031)				

Table 6. Component of Eq. (4)

Variable	Constant	Constant	Constant	Constant	Constant
A(×1)	-a0(2.378)	-b1(0.421)	-c1(0.0879)	-d1(0.0241)	-e1(0.525)
B(×2)	-a1(0.086)	-b2(0.214)	-c2(185.6)	-d2(0.0309)	-e2(0.297)
C(×3)	-a2(0.568)	-b3(0.386)	-c3(0.0461)	-d3(0.0169)	-e3(0.228)
D(×4)	-a3(0.189)	-b4(0.134)	-c4(0.0849)	-d4(0.0101)	
E(×5)	-a4(0.671)				

Table 7. Taguchi L16 orthogonal array of designed experiments

	Factors					Response	
Level	Reinforcement (g)	Contact Stiffness (μN/nm)	Max Force(μN)	Max Depth(nm)	Contact Area(nm^2)	Hardness(Gpa)	Er(Gpa)
1	0.2	7.8	179.0	124.2	5.99	0.303	2.810
2	0.2	6.5	185.6	92.2	3.48	0.540	3.170
3	0.2	5.5	147.2	289.3	3.06	0.400	2.840
4	0.2	1.3	113.6	468.7	6.54	0.171	2.790
5	0.4	7.8	185.6	289.3	6.54	0.279	2.670
6	0.4	6.5	179.0	468.7	3.06	0.500	3.360
7	0.4	5.5	113.6	124.2	3.48	0.300	2.602
8	0.4	1.3	147.2	92.2	5.99	0.200	0.460
9	0.6	7.8	147.2	468.7	3.48	0.400	3.690
10	0.6	6.5	113.6	289.3	5.99	0.200	2.340
11	0.6	5.5	179.0	92.2	6.54	0.260	1.900
12	0.6	1.3	185.6	124.2	3.06	0.604	0.670
13	0.4	7.8	113.6	92.2	3.06	0.370	4.030
14	0.4	6.5	147.2	124.2	6.54	0.220	0.860
15	0.4	5.5	185.6	468.7	5.99	0.309	2.060
16	0.4	1.3	179.0	289.3	3.48	0.514	0.610

4.10.3 Analysis of Variance and Percentage Contribution

An analysis of variance (ANOVA) was conducted to assess the statistical significance of each parameter. ANOVA can be employed for a quantitative study of control factors and their impact on the properties of the end product. This analysis helps determine the percentage contribution of control factors to the hardness and elastic modulus (Er) of the products.

The ANOVA analysis results indicate that the contact area (measured in nm^2) is a significant factor in the process of determining hardness., with a contribution of 67%, followed by max force(μN)with a contribution of 28%, but considered Contact stiffness(μN/nm), reinforcement content (g) and max depth (nm^2) not significantly factor with contribution (2.8%) (0.8%), (0.1%) respectively illustrated that in (Table 8).

The results indicate that the mechanical properties, specifically hardness, are mostly influenced by the contact area (measured in nm^2) and maximum force (measured in μN) [36]. therefore, can be negligible contact stiffness, reinforcement content (g) and max depth(nm), from the model because not significantly factor, the model became as in Eq. (7):

$$\begin{aligned}\text{Hardness (Gpa)} = {} & b1\times 2\_3.06 + b2\times 2\_3.48\\ & - b3\times 2\_5.99 - b4\times 2\_6.54\\ & - c1\times 3\_113.6 - c2\times 3\_147.2\\ & + c3\times 3\_179.0 + c4\ \times 3\_185.6\end{aligned} \quad (7)$$

The ANOVA analysis results for the elastic modulus (Er) reveal that contact stiffness is a crucial factor in the process, contributing significantly at 50%. Following this, the maximum depth (nm) contributes 17%, while the contact area (nm^2) is not considered a significantly influential factor, with a contribution of 9%. Other factors such as maximum force (µN) and reinforcement content (g) contribute 12% and 10%, respectively, as illustrated in Table 9. These results for elastic modulus Er are being more influenced by the contact stiffness (µN/nm) and max depth (nm) [38], therefore can be negligible, contact area (nm^2), max force (µN) and reinforcement content (g) from the model because not significantly factor the model became as Eq. (8):

$$\begin{aligned} \mathrm{Er} = {} & a1 \times 1\_92.2 - a2 \times 1\_124.2 - a3 \times 1\_289.3 \\ & + a4 \times 1\_468.7 - d1 \times 4\_1.3 \\ & + d2 \times 4\_5.5 + d3 \times 4\_6.5 \\ & + d4 \times 4\_7.8 \end{aligned} \tag{8}$$

Table 8. Illustrated Analysis of Variance for Hardness (Gpa)

Source	DF	Adj SS	Adj MS	F-Value	P-Value	Contribution %
Max depth (nm)	3	0.000463	0.000154	0.07	0.968	0.1%
Contact area(nm^2)	3	0.180303	0.060101	26.78	0.141	67.1%
Max force(µN)	3	0.075652	0.025217	11.24	0.215	28.2%
Contact stiffness(µN/nm)	3	0.007690	0.002563	1.14	0.582	2.8%
Reinforcement(g)	2	0.002475	0.001237	0.55	0.690	0.82%
Error	1	0.002245	0.002245			
Total	15	0.268828				

Table 9. Analysis of Variance for Er

Source	DF	Adj SS	Adj MS	F-Value	P-Value	Contribution %
Max depth nm	3	3.2662	1.0887	3.71	0.360	17.1%
Contact area(nm^2)	3	1.7377	0.5792	1.97	0.472	9.1%
Max force(µN)	3	2.2632	0.7544	2.57	0.423	11.88%
Contact stiffness(µN/nm)	3	9.5324	3.1775	10.83	0.219	50.1%
Reinforcement(g)	2	1.9237	0.9619	3.28	0.364	10.1%
Error	1	0.2934	0.2934			
Total	15	19.0166				

4.10.4 Estimating the performance properties in optimal conditions

The distribution of data can be effectively analyzed and modelled using a linear regression equation. A statistical model is developed utilizing linear regression equations by using Taguchi's orthogonal array and MINITAB software. Each material combination test is represented using a linear regression equation that accounts for all of the constituent parts. To determine the necessary outcomes and percentage of variability, the values of the response test combinations for the hardness test are calculated using the linear regression equation. For every test, Figure 15 shows the residual errors together with the associated R-square values. On the other hand, it is noted that the hardness response may be measured with the same set of conditions and provide a value of 98.21%. As a consequence, the outcome suggests that the parameters are statistically appropriate for the optimization study [8, 39].

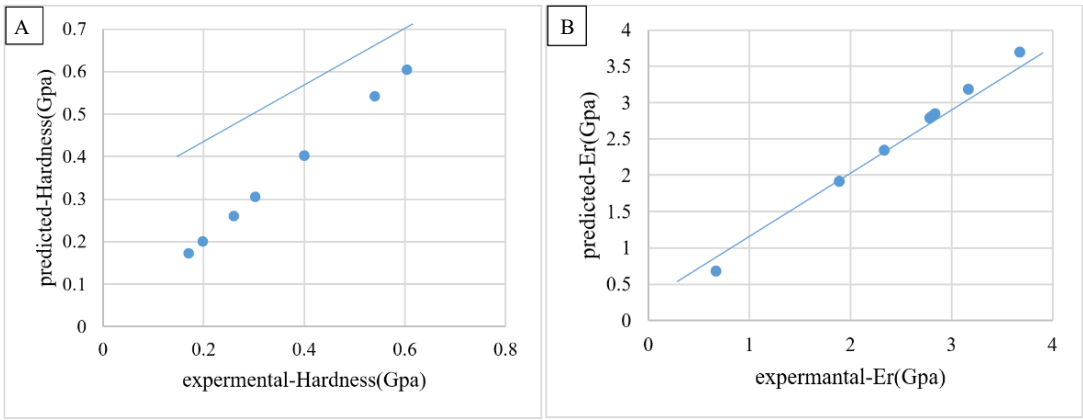

Figure 15. (A) Regression prediction plots of hardness (Gpa); (B) Regression prediction plots of elastic modulus (Gpa)

4.10.5 Response surface plot of hardness

The 3-D surface plots in Figure 16 illustrate the combined impact of reinforcement content (g), contact stiffness (µN/nm), maximum force (µN), contact area (nm^2), and maximum depth (nm). When calculating the optimal values for these variables, a crucial factor to take into account is the surface response. remarkably, all surface plots exhibit convex forms, indicating that the independent variables are carefully chosen. As indicated by a p-value<0.05, it is found that increasing the contact area (nm^2) and Max force (µN) significantly has affected hardness. A smaller hardness is obtained when a high contact area (6.45nm^2,) while a lower Max force (113µN) was obtained this is illustrated in Figure 16 (A). while in Figure 16 (B) obtained smaller hardness (0.2) with contact area(6.45nm^2),

contact stiffness (7.8μN/nm).

Whereas can be obtained higher value for Er (4.03Gpa), with Max depth (92.2nm) and contact stiffness(7.8μN/nm) this is illustrated in Figure16 (C), in Figure 16 (D) optimum value of elastic modulus Er (3.69Gpa) vs max depth(469nm), contact stiffness (7.8 μN/nm) [40].

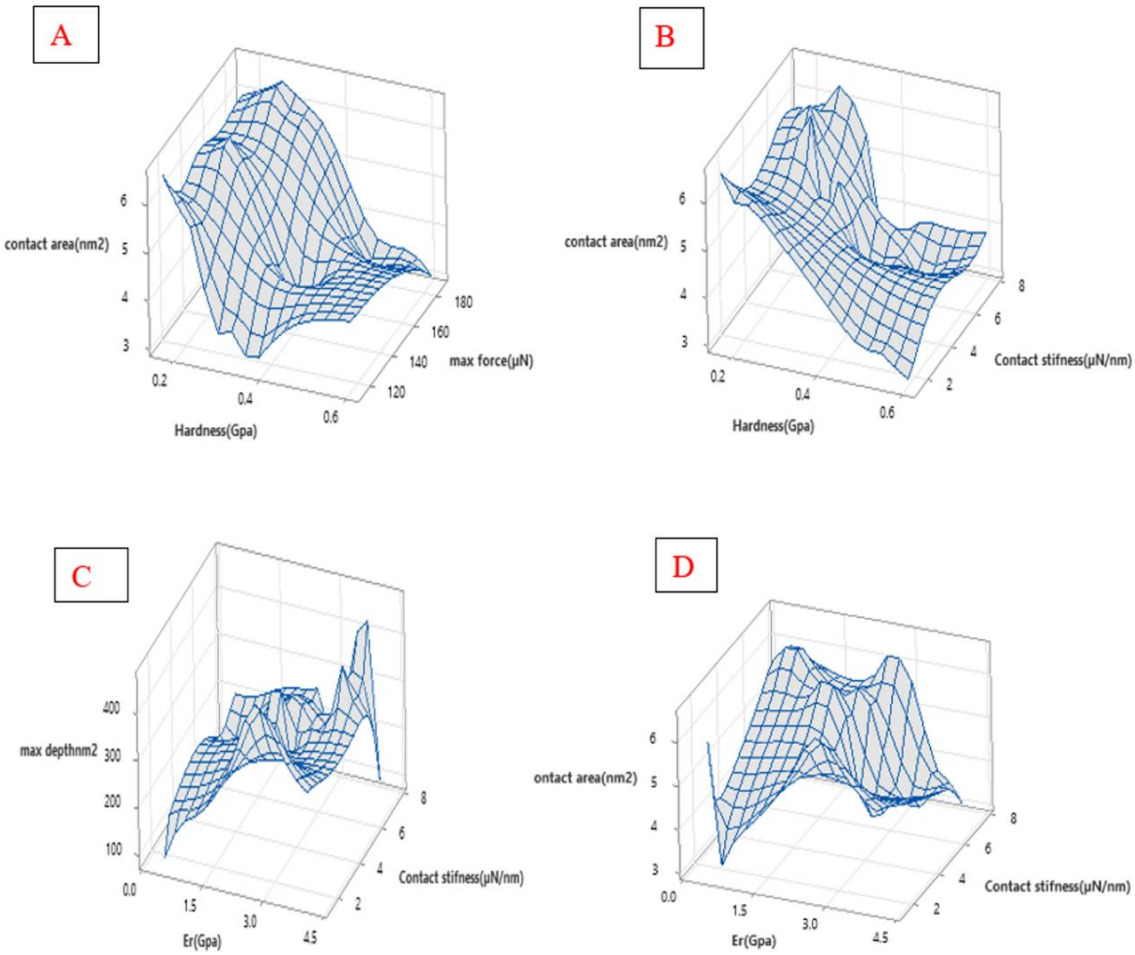

Figure 16. A) surface plot of hardness (Gpa) vs contact area (nm^2), max force (μN); B) surface plot of hardness (Gpa) vs contact area (nm^2), contact stiffness (μN/nm); C) surface plot of elastic modulus Er (Gpa) vs max depth(nm), Contact stiffness (μN/nm); D) surface plot of elastic modulus Er (Gpa) vs contact stiffness, contact stiffness (μN)

5. CONCLUSIONS

This study showed the production of a nanofiber membrane using the electrospinning method. This nanofiber membrane is created by combining 80% polyvinyl alcohol (PVA), 20% chitosan (CS), and reinforcing it with titanium dioxide (TiO_2) nanoparticles at three different concentrations. Additionally, the membrane contains the antibacterial medication rifampicin (RIF). The membrane obtained from this study had excellent biocompatibility and was found to have a diameter of 276nm and a pore size of 836nm. Furthermore, the membrane showed an inhibition zone diameter of 20mm for the PVA/CS/0.4TiO_2+RIF composition. These results were observed during the study. The cell viability remained above 85% for 24 hours at all tested concentrations, indicating that the composite nanofibers are non-toxic and exhibit good biocompatibility with cells. This was assessed by cultivating the cells on thin scaffolds. After five days, the membranes grown with the cells have exhibited a uniform and fully covered surface through a nanoindentation test to determine their mechanical properties. This test has revealed the development of mechanical reinforcement by incorporating nanoparticles, resulting in a composite nanofiber mat that holds great potential as a material for wound dressings.

The Taguchi technique is used to select the optimal combination of four parameters that affect the mechanical properties of (PVA/CA/TiO_2): reinforcement content (g), stiffness content (μN/nm), max force (μN), and max depth (nm). The Taguchi model is used to optimise these parameters at four levels, and their impact on hardness is assessed. The contact area (measured in nm^2) plays an important role in the process, accounting for 67% of the observed variations in hardness, as shown by the ANOVA analysis. The maximum force (measured in μN) contributes 28% to the observed variations, while the contribution of the elastic modulus is not specified. It is demonstrated that contact stiffness is a significant factor in the process, contributing 50% to the outcome.

The maximum depth (measured in nanometers) follows with a contribution of 17%. By using this procedure, it is possible to optimize the most influential factor on the mechanical properties of wound dressing materials, ensuring they are suitable and comfortable. Additionally, these materials exhibit antibacterial, wound healing, biocompatible, and hem compatible properties due to the presence of CS/PVA/TiO_2 can be suggested for future study with the developed composite scaffolds are:

1) Use of poly (ε-caprolactone) /chitosan with collagen–blend for skin generation.
2) Prepare Polyurethane (PU) with Chitosan Scaffolds

for Tissue Engineering by using another technique such as solvent casting.

3) Similar studies in vivo using animal models to determine the feasibility of these strategies for clinic application.
4) Using of different bioactive ratios for bio composite membrane.

ACKNOWLEDGEMENT

"Thanks for laboratories of Materials Engineering, University of Technology-Iraq, Baghdad."

REFERENCES

[1] Winkler, M.A., Dib, C., Ljubimov, A.V., Saghizadeh, M. (2014). Targeting miR-146a to treat delayed wound healing in human diabetic organ-cultured corneas. PloS One, 9(12): e114692. https://doi.org/10.1371/journal.pone.0114692

[2] Jayarama Reddy, V., Radhakrishnan, S., Ravichandran, R., Mukherjee, S., Balamurugan, R., Sundarrajan, S., Ramakrishna, S. (2013). Nanofibrous structured biomimetic strategies for skin tissue regeneration. Wound Repair and regeneration, 21(1): 1-16. https://doi.org/10.1111/j.1524-475X.2012.00861.x

[3] Iqbal, N., Khan, A.S., Asif, A., Yar, M., Haycock, J.W., Rehman, I.U. (2019). Recent concepts in biodegradable polymers for tissue engineering paradigms: A critical review. International Materials Reviews, 64(2): 91-126. https://doi.org/10.1080/09506608.2018.1460943

[4] Zhang, J., Xia, W., Liu, P., Cheng, Q., Tahirou, T., Gu, W., Li, B. (2010). Chitosan modification and pharmaceutical/biomedical applications. Marine Drugs, 8(7): 1962-1987. https://doi.org/10.3390/md8071962

[5] Qiu, K., Netravali, A.N. (2013). A composting study of membrane-like polyvinyl alcohol based resins and nanocomposites. Journal of Polymers and the Environment, 21: 658-674. https://doi.org/10.1007/s10924-013-0584-0

[6] Ko, S.W., Lee, J.Y., Lee, J., Son, B.C., Jang, S.R., Aguilar, L.E., Oh, Y.M., Park, C.H., Kim, C.S. (2019). Analysis of drug release behavior utilizing the swelling characteristics of cellulosic nanofibers. Polymers, 11(9): 1376. https://doi.org/10.3390/polym11091376

[7] Augustine, R., Malik, H.N., Singhal, D.K., Mukherjee, A., Malakar, D., Kalarikkal, N., Thomas, S. (2014). Electrospun polycaprolactone/ZnO nanocomposite membranes as biomaterials with antibacterial and cell adhesion properties. Journal of Polymer Research, 21: 1-17. https://doi.org/10.1007/s10965-013-0347-6

[8] Mohammed Zayan, J., Rasheed, A.K., John, A., Khalid, M., Ismail, A.F., Aabid, A., Baig, M. (2021). Investigation on rheological properties of water-based novel ternary hybrid nanofluids using experimental and taguchi method. Materials, 15(1): 28. https://doi.org/10.3390/ma15010028

[9] Natrayan, L., Kumar, P.A., Baskara Sethupathy, S., Sekar, S., Patil, P.P., Velmurugan, G., Thanappan, S. (2022). Effect of nano TiO_2 filler addition on mechanical properties of bamboo/polyester hybrid composites and parameters optimized using grey Taguchi method. Adsorption Science & Technology, 2022: 6768900. https://doi.org/10.1155/2022/6768900

[10] Kadhim, I.A., Ameer, Z.J.A., Alzubaidi, A.B. (2020). Investigation of chitosan film degradation in tissue engineering applications. In IOP Conference Series: Materials Science and Engineering. IOP Publishing, 671(1): 012060. https://doi.org/10.1088/1757-899X/671/1/012060

[11] Bahjat, H.H., Ismail, R.A., Sulaiman, G.M., Jabir, M.S. (2021). Magnetic field-assisted laser ablation of titanium dioxide nanoparticles in water for anti-bacterial applications. Journal of Inorganic and Organometallic Polymers and Materials, 31(9): 3649-3656. https://doi.org/10.1007/s10904-021-01973-8

[12] Khashan, K.S., Badr, B.A., Sulaiman, G.M., Jabir, M.S., Hussain, S.A. (2021). Antibacterial activity of Zinc Oxide nanostructured materials synthesis by laser ablation method. In Journal of Physics: Conference Series. IOP Publishing, 1795(1): 012040. https://doi.org/10.1088/1742-6596/1795/1/012040

[13] Mohammed, M.K., Mohammad, M.R., Jabir, M.S., Ahmed, D.S. (2020). Functionalization, characterization, and antibacterial activity of single wall and multi wall carbon nanotubes. In IOP Conference Series: Materials Science and Engineering. IOP Publishing, 757(1): 012028. https://doi.org/10.1088/1757-899X/757/1/012028

[14] Nematollahi, Z., Tafazzoli-Shadpour, M., Zamanian, A., Seyedsalehi, A., Mohammad-Behgam, S., Ghorbani, F., Mirahmadi, F. (2017). Fabrication of chitosan silk-based tracheal scaffold using freeze-casting method. Iranian Biomedical Journal, 21(4): 228. https://doi.org/10.18869%2Facadpub.ibj.21.4.228

[15] Zhao, R., Li, X., Sun, B., Zhang, Y., Zhang, D., Tang, Z., Chen, X., Wang, C. (2014). Electrospun chitosan/sericin composite nanofibers with antibacterial property as potential wound dressings. International Journal of Biological Macromolecules, 68: 92-97. https://doi.org/10.1016/j.ijbiomac.2014.04.029

[16] Javanmardi, S., Divband, B. (2018). Titanium dioxide nanoparticle/gelatin: A potential burn wound healing biomaterial. Wounds: A Compendium of Clinical Research and Practice, 30(12): 372-379.

[17] Gruppuso, M., Guagnini, B., Musciacchio, L., Bellemo, F., Turco, G., Porrelli, D. (2022). Tuning the drug release from antibacterial polycaprolactone/rifampicin-based core-shell electrospun membranes: A proof of concept. ACS Applied Materials & Interfaces, 14(24): 27599-27612. https://doi.org/10.1021/acsami.2c04849

[18] Skarmoutsou, A., Lolas, G., Charitidis, C.A., Chatzinikolaidou, M., Vamvakaki, M., Farsari, M. (2013). Nanomechanical properties of hybrid coatings for bone tissue engineering. Journal of The Mechanical Behavior of Biomedical Materials, 25: 48-62. https://doi.org/10.1016/j.jmbbm.2013.05.003

[19] Jabir, M.S., Rashid, T.M., Nayef, U.M., Albukhaty, S., AlMalki, F.A., Albaqami, J., AlYamani, A.A., Taqi, Z.J., Sulaiman, G.M. (2022). Inhibition of Staphylococcus aureus α-hemolysin production using nanocurcumin capped Au@ ZnO nanocomposite. Bioinorganic Chemistry and Applications, 2022(1): 2663812. https://doi.org/10.1155/2022/2663812

[20] Singh, K.R., Nayak, V., Singh, R.P. (2021). Introduction to bionanomaterials: An overview. Bionanomaterials:

Fundamentals and Biomedical Applications, pp. 1-21. https://doi.org/10.1088/978-0-7503-3767-0ch1
[21] Baghali, M., Ziyadi, H., Faridi-Majidi, R. (2022). Fabrication and characterization of core-shell TiO_2-containing nanofibers of PCL-Zein by coaxial electrospinning method as an erythromycin drug carrier. Polymer Bulletin, 79: 1729-1749. https://doi.org/10.1007/s00289-021-03591-3
[22] Jasim, T.Y., Najim, M.A., Jabur, A.R. (2019). Improving the mechanical properties of (chitosan/polyurethane) electrospun blend scaffold used for skin regeneration. In AIP Conference Proceedings. AIP Publishing, 2123(1). https://doi.org/10.1063/1.5116969
[23] Jabur, A.R., Al-Hassani, E.S., Al-Shammari, A.M., Najim, M.A., Hassan, A.A., Ahmed, A.A. (2017). Evaluation of stem cells' growth on electrospun polycaprolactone (PCL) scaffolds used for soft tissue applications. Energy Procedia, 119: 61-71. https://doi.org/10.1016/j.egypro.2017.07.048
[24] Ali, I.H., Jabir, M.S., Al-Shmgani, H.S., Sulaiman, G.M., Sadoon, A.H. (2018). Pathological and immunological study on infection with Escherichia coli in ale balb/c mice. In Journal of Physics: Conference Series. IOP Publishing, 1003: 012009. https://doi.org/10.1088/1742-6596/1003/1/012009
[25] Younus, A., Al-Ahmer, S., Jabir, M. (2019). Evaluation of some immunological markers in children with bacterial meningitis caused by Streptococcus pneumoniae. Research Journal of Biotechnology, 14: 131-133.
[26] Ismail, N.A., Amin, K.A.M., Majid, F.A.A., Razali, M.H. (2019). Gellan gum incorporating titanium dioxide nanoparticles biofilm as wound dressing: Physicochemical, mechanical, antibacterial properties and wound healing studies. Materials Science and Engineering: C, 103: 109770. https://doi.org/10.1016/j.msec.2019.109770
[27] Kadhim, I.A.U., Sallal, H.A., Al-Khafaji, Z.S. (2023). A review in investigation of marine biopolymer (chitosan) for bioapplications. ES Materials & Manufacturing, 21: 828. http://dx.doi.org/10.30919/esmm5f828
[28] Niranjan, R., Kaushik, M., Selvi, R.T., Prakash, J., Venkataprasanna, K.S., Prema, D., Pannerselvam, B., Venkatasubbu, G.D. (2019). PVA/SA/TiO_2-CUR patch for enhanced wound healing application: In vitro and in vivo analysis. International Journal of Biological Macromolecules, 138: 704-717. https://doi.org/10.1016/j.ijbiomac.2019.07.125
[29] Hou, J., Dong, G., Luu, B., Sengpiel, R.G., Ye, Y., Wessling, M., Chen, V. (2014). Hybrid membrane with TiO_2 based bio-catalytic nanoparticle suspension system for the degradation of bisphenol-A. Bioresource Technology, 169: 475-483. https://doi.org/10.1016/j.biortech.2014.07.031
[30] Behera, S.S., Das, U., Kumar, A., Bissoyi, A., Singh, A.K. (2017). Chitosan/TiO_2 composite membrane improves proliferation and survival of L929 fibroblast cells: Application in wound dressing and skin regeneration. International Journal of Biological Macromolecules, 98: 329-340. https://doi.org/10.1016/j.ijbiomac.2017.02.017
[31] Kim, J.I., Kim, C.S. (2018). Harnessing nanotopography of PCL/collagen nanocomposite membrane and changes in cell morphology coordinated with wound healing activity. Materials Science and Engineering: C, 91: 824-837. https://doi.org/10.1016/j.msec.2018.06.021
[32] Yang, Y., Zhang, R., Liang, Z., Guo, J., Chen, B., Zhou, S., Yu, D. (2024). Application of electrospun drug-loaded nanofibers in cancer therapy. Polymers, 16(4): 504. https://doi.org/10.3390/polym16040504
[33] Baghaie, S., Khorasani, M.T., Zarrabi, A., Moshtaghian, J. (2017). Wound healing properties of PVA/starch/chitosan hydrogel membranes with nano Zinc oxide as antibacterial wound dressing material. Journal of Biomaterials Science, Polymer Edition, 28(18): 2220-2241. https://doi.org/10.1080/09205063.2017.1390383
[34] Hussain, W.S., Hamad, Q.A., Oleiwi, J.K. (2023). Mechanical and numerical analysis of polymer-natural fiber composites for denture applications. Revue des Composites et des Matériaux Avancés-Journal of Composite and Advanced Materials, 33(4): 233-242, https://doi.org/10.18280/rcma.330404
[35] Lu, X.L., LÜ, X.Q., Wang, J.Y., Sun, Z.J., Tong, Y.X. (2013). Preparation and shape memory properties of TiO_2/PLCL biodegradable polymer nanocomposites. Transactions of Nonferrous Metals Society of China, 23(1): 120-127. https://doi.org/10.1016/S1003-6326(13)62437-1
[36] Mairpady, A., Mourad, A.H.I., Mozumder, M.S. (2021). Statistical and machine learning-driven optimization of mechanical properties in designing durable HDPE nanobiocomposites. Polymers, 13(18): 3100. https://doi.org/10.3390/polym13183100
[37] Macías, H.A., Yate, L., Coy, E., Aperador, W., Olaya, J.J. (2021). Insights and optimization of the structural and mechanical properties of TiWSiN coatings using the taguchi method. Applied Surface Science, 558: 149877. https://doi.org/10.1016/j.apsusc.2021.149877
[38] Muluh, N.S., Tamungang, N.E.B., Ghogomu, J.N., Noufame, T.D. (2021). Pt, N co-doped TiO_2 ternary nanocomposite associated with activated carbon for the photocatalytic degradation of Methylene blue: Optimization and modeling using the taguchi design. International Journal of Chemical Science, 5(4): 29-38,
[39] Daassi, R., Durand, K., Rodrigue, D., Stevanovic, T. (2023). Optimization of the electrospray process to produce lignin nanoparticles for PLA-based food packaging. Polymers, 15(13): 2973. https://doi.org/10.3390/polym15132973
[40] Hussein, A.K., Abbas, L.K., Dawood, J.J. (2016). Multiple objective optimization of weld geometry of dissimilar metals. 16: 418-434.

NOMENCLATURE

ANOVA	Analysis of variance
CS	Chitosan
CA	Contact angle
DOE	Design of experimental
EDX	Energy dispersion x-ray spectroscopy
FTIR	Fourier transform infrared spectroscopy
FESEM	Field emotion scanning electron microscopy
PVA	Polyvinyl alcohol
PBS	Phosphate buffer saline
W0	The dry weight before degradation

Wd	Dry weight after degradation at the specified time	DSC	Differential scanning calorimetry
		XRD	X-ray diffraction
TiO_2	Titanium dioxide	HRTE	High-resolution transmission electron microscopy
RIF	Rifampicin as an Antibiotics		
WVTR	Water vapours transfer rate	WVTR	Water vapours transfer rate
NPs	Nano particles		